ISSN 1027-4510, Journal of Surface Investigation. X-ray, Synchrotron and Neutron Techniques, 2015, Vol. 9, No. 5, pp. 1099–1106. © Pleiades Publishing, Ltd., 2015.

Removal of a Lead Film from Graphene by Xenon-Beam Bombardment: Computer Experiment

A. E. Galashev[a] and V. A. Polukhin[b]

[a] *Institute of High Temperature Electrochemistry, Ural Branch, Russian Academy of Sciences, Yekaterinburg, 620219 Russia*
e-mail: alexander-galashev@yandex.ru

[b] *Institute of Materials Science and Metallurgy, Yeltsin Ural Federal University, Yekaterinburg, 620002 Russia*

Received January 22, 2015

Abstract—The process of the bombardment of a Pb film on modified graphene at an incident angle of 75° in the range of Xe_{13} cluster energies of 5 to 30 eV is studied using the molecular dynamics method. The modification includes the creation of divacancies located approximately uniformly over the graphene sheet, as well as hydrogenation of the graphene edges and the partial hydrogenation of divacancy boundaries. The horizontal and vertical components of the self-diffusion coefficient of the lead film and graphene, stresses on the horizontal metal and graphene surfaces, the angular distribution of the nearest geometric neighbors in graphene, and the roughness of the graphene-sheet surface during Xe_{13} cluster bombardment of a target are calculated. The graphene was completely purified of lead only under 30-eV Xe_{13} cluster impacts. The separation of lead from graphene was predominantly collective. None of the bombardments leads to serious damage to the graphene.

Keywords: bombardment, graphene, xenon cluster, molecular dynamics, lead

DOI: 10.1134/S1027451015050274

INTRODUCTION

The possibility of synthesizing large-area graphene films on metals using the method of chemical-vapor deposition has aroused significant interest in studying the metal–graphene interface [1]. In these cases, the metal acts as a catalyst for the complete dehydrogenation of hydrocarbon precursors in order to extract carbon to the surface. In the case of metals with a low reactivity, the method of physical carbon vapor deposition can be used to synthesize graphene [2, 3]. Depending on the metal type and the temperature, carbon diffuses into the bulk during graphene growth. The amount of carbon in the bulk depends on the carbon solubility in the metal. This property is important for determination of whether graphene can grow on a metal surface at high temperatures. Materials that dissolve a large amount of carbon in the bulk can also deposit a significant amount of carbon on the surface during cooling. Thermodynamically controlled deposition can be controlled kinetically to a certain extent, for example, by fast cooling. Carbon is almost insoluble in hard lead. However, lead carbonate can be obtained by running CO_2 through a cold dilute lead–acetate solution or by shaking a lead-salt suspension, which is less soluble than a carbonate, with ammonium carbonate at a low temperature. Under ion bombardment, lead films can be heated considerably, which enhances its adhesion to graphene. If the relatively low melting temperature of Pb (T_m = 600 K) is taken into account, it can be suggested that the removal of the Pb film from graphene via bombardment with noble-gas clusters occurs differently than in the case of the removal of a Cu film of the same type [4–7].

Low-energy ion beams are used as a tool for surface growth and etching in some methods for treating surfaces [8, 9]. Molecular dynamics (MD) simulation using Ar ions obliquely incident on a Si (001) surface (with an incidence angle of 45°) revealed the presence of significant displacements of surface atoms even at energies smaller than 20 eV [10]. Using the MD method, the authors of [11] studied defect formation under 25–800-eV Si atom beam bombardment of a Si (001) surface. They obtained the depth dependence of the surface damage on the projectile energies and the bombardment duration. The polymer surfaces were purified most effectively as a result of 10-keV C_{60} ion-beam bombardment at incident angles of 75° [12].

It is possible to remove negligibly small amounts of heavy metals from air and water using filters with graphene membranes. The problem of purifying filters of the metal sediment arises in this case. Lead has a low energy of adhesion to perfect graphene (0.2 eV) [13]; however, the energy of Pb coupling to graphene at the divacancy boundary is very appreciable (3.4 eV) [14]. It was shown experimentally that, in the case of Xe atom incidence on a graphite surface at an angle of 55°, phonon surface modes obtain more transferred

energy (by 20%) than in the case of a vertically directed beam. It was shown that a Xe atom is scattered on the smooth graphite surface even at energies of several tens of electronvolts. To decrease the probability of damaging graphene under the bombardment of a lead–graphene film, we chose an incidence angle of 75°. The energies of cluster beams used are much smaller than those in experiments the main problem of which was sputtering of the bombarded material.

The aim of this paper is to thoroughly study the process of lead film removal from partially hydrogenated imperfect graphene without damaging it.

COMPUTER MODEL

The interatomic interactions in graphene were represented using the Tersoff many-body potential [16]. This potential is based on the concept of binding order. The potential energy between the neighboring atoms i and j is written as

$$V_{ij} = f_C(r_{ij})\left[A\exp(-\lambda^{(1)}r_{ij}) - Bb_{ij}\exp(-\lambda^{(2)}r_{ij})\right], \quad (1)$$

$$f_C(r_{ij}) = \begin{cases} 1, \\ \frac{1}{2} + \frac{1}{2}\cos\left[\pi\left(r_{ij} - R^{(1)}\right)\Big/\left(R^{(2)} - R^{(1)}\right)\right], \\ 0 \end{cases} \quad \begin{array}{c} r_{ij} < R^{(1)}, \\ R^{(1)} < r_{ij} < R^{(2)}, \\ r_{ij} > R^{(2)}, \end{array} \quad (2)$$

where b_{ij} is the many-body binding-order parameter describing the creation of the bond-formation energy (the attractive part V_{ij}) for the local atomic arrangement because of the presence of other neighboring atoms. The potential energy is a many-body function of the positions of atoms i, j, and k and is determined by the parameters

$$b_{ij} = (1 + \beta^n \xi_{ij}^{n_i})^{-1/(2n)}, \quad (3)$$

$$\xi_{ij} = \sum_{k\neq i,j} f_C(r_{ij})g(\theta_{ijk}), \quad (4)$$

$$g(\theta_{ijk}) = 1 + \frac{c^2}{d^2} - \frac{c^2}{\left[d^2 + (h - \cos\theta_{ijk})^2\right]}, \quad (5)$$

where ξ is the effective coordination number, $g(\theta_{ijk})$ is the function of the angle between r_{ij} and r_{ik}, which stabilizes the structure of the tetrahedron.

The covalent bond distance was increased to 0.23 nm, and additional weak attraction given by the Lennard-Jones potential with the parameters in [17] was included for $r > 0.23$ nm. To remove the resulting rotating moment at each site of the graphene sheet, we excluded the rotating component of the force produced by atoms at adjoining sites. The analytical form of the local torsional interaction potential was given in [17].

To simulate atomic interactions in a Pb film, we used the Sutten–Chen many-body potential [18]. The Sutten–Chen potential energy is written as

$$U^{SC} = \varepsilon\left[\frac{1}{2}\sum_i\sum_{j\neq i} V(r_{ij}) - c\sum_i \sqrt{\rho_i}\right], \quad (6)$$

where

$$V(r_{ij}) = (a/r_{ij})^q, \quad \rho_i = \sum_{j\neq i}(a/r_{ij})^s. \quad (7)$$

Here, ε is the parameter with the dimensions of energy; c is a dimensionless parameter; a is the parameter with the dimensions of length, which is usually chosen to be equal to the lattice constant; and q and s are positive integers, $q > s$.

The power-law forms of the contributions make it possible to successfully combine short-range interactions, which are represented by the N-particle term, and the van der Waals "tail," which is determined by long-range interaction.

The lead–carbon and xenon–xenon interactions were given by the Lennard-Jones potential [19–21]. The interaction between the Xe atoms and target atoms (Pb and C) was defined by the purely repulsive ZBL potential [22]:

$$\begin{aligned}\Phi = {} & Z_i Z_j \frac{e^2}{r}\left\{0.1818\exp\left(-3.2\frac{r}{a}\right)\right. \\ & + 0.5099\exp\left(-0.9423\frac{r}{a}\right) \\ & + 0.2802\exp\left(-0.4029\frac{r}{a}\right) \\ & \left. + 0.02817\exp\left(-0.2016\frac{r}{a}\right)\right\}.\end{aligned} \quad (8)$$

Here, Z_i and Z_j are the atomic numbers of the ith and jth atoms, e is the elementary electric charge, r is the distance between atoms, and parameter a is determined by the following expression:

$$a = 0.8854a_0\left(Z_i^{0.23} + Z_j^{0.23}\right)^{-1}, \quad (9)$$

where a_0 is the Bohr radius. We disregard the weak attraction between Xe and Pb atoms and also between the Xe and C atoms, because the primary aim of this study lies in investigating the transfer of energy and angular momentum rather than chemical binding [23].

Defects enhance the adhesion of metals to graphene considerably. Divacancies are most frequent defects in graphene. The graphene sheet used to deposit lead had four divacancies rather uniformly distributed over its surface. Hydrogenation was used to strengthen the divacancy edges and boundaries. The CH groups formed at the edges and sites nearest to the divacancy center were simulated in accordance with

the single-atom scheme [24]. The C–CH and CH–CH interactions were represented in terms of the Lennard-Jones potential [24]. The partial functionalization of graphene in the form of the attachment of hydrogen atoms to its edges stabilizes the structure without increasing the interatomic distances and without producing roughness on the entire surface.

The Pb film on graphene was formed in a separate MD calculation consisting of two stages. In the first stage, Pb atoms were placed above centers of nonadjacent graphene cells so that the distance between the Pb atoms and C atoms was equal to 2.33 Å, which was calculated in accordance with density functional theory [14]. 51 Pb atoms were deposited onto this friable Pb film consisting of 49 atoms. Then a system consisting of 100 Pb atoms and 406 C atoms was brought into a state of equilibrium in the MD calculation in 1 million time steps ($\Delta t = 0.2$ fs). The equations were solved numerically using the Runge–Kutta method of the fourth order. The model obtained in such a way was bombarded with icosahedral Xe_{13} clusters. Five starting points for the location of the Xe_{13} cluster centers were distributed uniformly on one line parallel to the *oy* axis (the "armchair" direction). This line was shifted to the left (along the *ox* axis) from the left graphene edge by a distance of 1.5 nm and was lifted by a height (in the *oz*-axis direction) such that the angle φ between the passage of the *ox* axis near the upper film surface and the impact-direction line was 15°. The interval equal to the graphene sheet length in the *ox*-axis direction (the "zigzag" direction) was divided into five equal segments with the length $L_i = L_x/5$. At the beginning of each subsequent cycle of cluster impacts, the line of the starting point of the Xe_{13} clusters was moved horizontally forward by the distance L_i. As a result, the film surface approximated by the plane was covered by 25 uniformly distributed points at which cluster impacts were aimed. Each series included 5 cycles or 25 impacts. At the starting point, all Xe_{13} cluster atoms acquired the same velocity determining the impact direction. Clusters in turn were sent to the target. The lifetime of each cluster (determined by the sum of its flight time and the time of its interaction with the target) was limited to 8 ps. After that period of time, Xe atoms of the broken cluster were excluded from consideration, and a new Xe_{13} cluster began its motion from another initial point. The duration of the cycle consisting of five cluster-bombardment events was 40 ps, that of the series (five cycles) was 0.2 ns (in what follows, the impact number will be denoted by *n*), and that of the entire bombardment (five series) was 1 ns. Bombardment for five cluster energies (5, 10, 15, 20, and 30 eV) was at an incident angle of $\theta = 75°$.

Cluster impact on the surface was accompanied by system heating. The liberated heat was removed from the system moderately using the Berendsen scheme with the coupling constant $\tau = 4$ fs [25]. To control heating, at each time step, the velocities ν were scaled in accordance with the expression

$$v = \lambda v, \quad \lambda = \left[1 + \frac{\Delta t}{\tau}\left(\frac{T_0}{T} - 1\right)\right]^{1/2}, \tag{10}$$

where λ is the scaling factor, T_0 is the chosen temperature (300 K), and T is the current temperature.

The coefficient of atom diffusion was calculated [26, 27] as follows:

$$D = D_{xy} + D_z = \frac{1}{2\Gamma\tau}\left\langle\left[\Delta\mathbf{r}(t)\right]^2\right\rangle_p, \tag{11}$$

where $\Gamma = 3$ is the spatial dimensionality. Averaging over p is denoted as $\langle\ldots\rangle$, where p is the number of time intervals used to determine $\left\langle\left[\Delta\mathbf{r}(t)\right]^2\right\rangle$. The five time dependences were averaged, each of them was calculated in an interval of $\tau = 200$ ps.

The stress in the position of the *i*th atom of the metal film was determined as follows [18]:

$$\sigma_{\alpha\beta}(i) = \frac{\varepsilon}{2a^2\Omega_i}\sum_{j\neq i}^{k}\Big[-q\left(a/r_{ij}\right)^{q+2} + cs\left(1/\sqrt{\rho_i} + 1/\sqrt{\rho_j}\right)\left(a/r_{ij}\right)^{s+2}\Big]r_{ij}^{\alpha}r_{ij}^{\beta}, \tag{12}$$

where the volume Ω_i related to an individual atom can be associated with that of the Voronoi polyhedron related to the atom *i*.

To calculate stresses appearing in graphene, the graphene sheet was divided into elementary areas. The atomic stresses $\sigma_{uJ}(l)$ on an elementary area with the orientation denoted by the subscript *u* and the number *l* for each of the directions *x*, *y*, and *z* with the current subscript *J* were determined by calculating the kinetic energies of atoms on this area and the projections of forces f_J^i acting on the *l*th area from all other atoms [28]:

$$\sigma_{uJ}(l) = \left\langle\sum_i^k\frac{1}{\Omega}\left(mv_J^i v_J^i\right)\right\rangle + \frac{1}{S_l}\left\langle\sum_i^k\left(f_J^i\right)\right\rangle, \tag{13}$$

where *k* is the number of atoms on the *l*th area, Ω is the volume per atom, *m* is the atomic mass, v_J^i is the *J*th projection of the velocity of the *i*th atom, and S_l is the area of the *l*th area. In the case of such determination, compressive stresses can have plus and minus signs in accordance with the directions of the forces f_J^i. This is the difference between the microscopic stress $\sigma_{uJ}(l)$ and the macroscopic one $\bar{\sigma}_J < 0$. The total stresses acting in the graphene plane were determined by summing the corresponding elementary stresses:

$$\sigma_{zJ} = \sum_{l=1}^{N_l}\sigma_J^z(l), \tag{14}$$

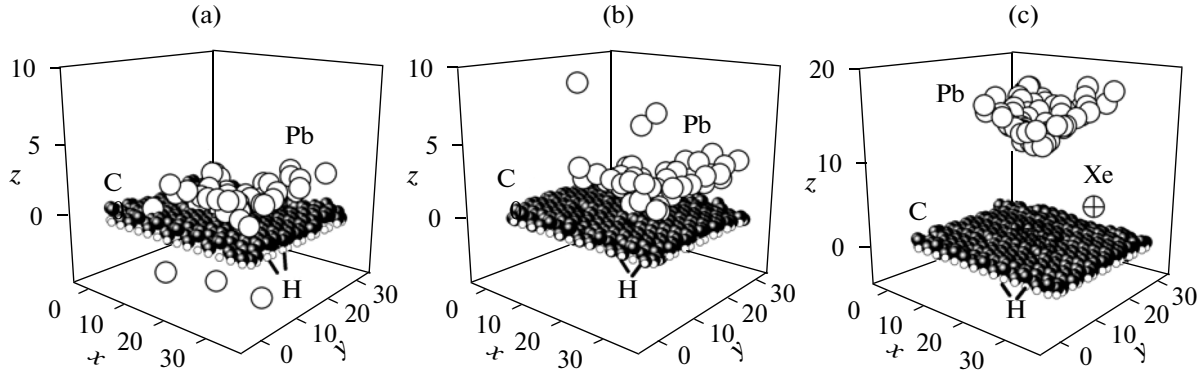

Fig. 1. Configuration of the "Pb film–partially hydrogenated graphene" system after bombardment at an incident angle of 75° with Xe_{13} cluster energies: (a) 10, (b) 20, and (c) 30 eV. The coordinates of atoms are given in angstroms.

where N_l is the number of elementary areas of division of the graphene sheet in the chosen direction.

The surface roughness (or the arithmetic mean profile deviation) was calculated as follows:

$$R_a = \frac{1}{N}\sum_{i=1}^{N}|z_i - \bar{z}|, \qquad (15)$$

where N is the number of sites (atoms) on the graphene surface, z_i is the level of the atom i, $\bar{z}$ is the graphene surface level, and z_i and $\bar{z}$ were determined at the same instants of time.

The total energy of free single-sheet graphene obtained at $T = 300$ K was -7.02 eV, which agrees with the quantum mechanical calculation (-6.98 eV) [29]. The melting temperature of the Pb_{201} cluster with a free surface determined in a separate calculation was 417 K, which agrees with the MD calculations (T_m = 412 K) [30] also carried out with the Sutton–Chen potential. In both cases, T_m was determined using a jump in the potential energy.

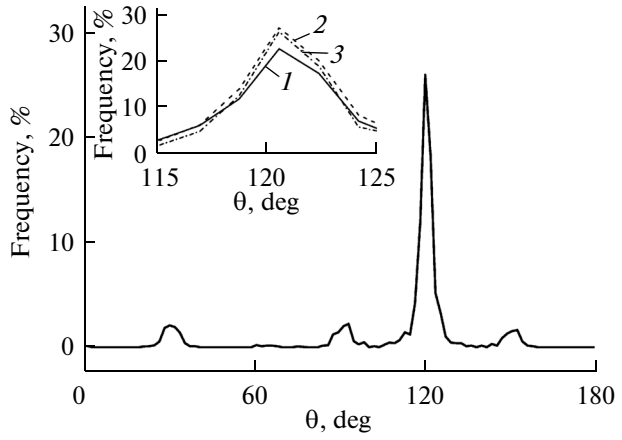

Fig. 2. Angular distribution of the nearest geometric neighbors in graphene obtained after 30-eV cluster beam bombardment of the target. The inset shows the main peaks (on a magnified scale) of the angular distributions after cluster bombardment with energies: (*1*) 10, (*2*) 20, and (*3*) 30 eV.

CALCULATION RESULTS

The configurations of the "Pb–graphene–H" film obtained after 125 impacts of Xe_{13} clusters with energies of 10, 20, and 30 eV are shown in Fig. 1. As can be seen from the figure, complete separation of the metal from graphene occurred only in the case of 30-eV cluster bombardment of the target. When the energy of the bombarding clusters was 10 eV, a fraction of Pb atoms was ejected from the film, but the majority of them remained on the graphene-sheet surface, where atoms embedded in bivacancies were present. Doubling of the energy of the bombarding Xe_{13} clusters (at E_{Xe} = 20 eV) retained the single knocking out of Pb atoms, and, in addition, allowed a shift in the film portion remaining on the graphene along its surface. In the case of a bombarding-cluster energy of 30 eV, the predominant mechanism for Pb separation from the graphene substrate was the flaking of a considerable film piece (cluster) rather than the knocking out of individual atoms. The separated portion of the Pb film had a cone-shaped form the vertex of which faced the graphene. Such a form was produced by impacts of Xe atoms reflected from graphene on the film surface adjoining the substrate. We note that the mechanism of the predominant single knocking out of Cu atoms dominated under Ar_{13} cluster bombardment of the Cu film on perfect graphene [4–7].

Even after impacts of 30-eV Xe_{13} clusters, the graphene sheet with hydrogenated edges was not subjected to any serious damage. The order of C-atom arrangement remained unchanged over the entire area of the graphene sheet, including the edges and in the vicinity of the divacancies. This was confirmed by the angular distribution of the nearest geometric neighbors in graphene obtained after 30-eV Xe cluster bombardment of the target (Fig. 2). There is one pointed peak located at an angle of 120° which reflects packing

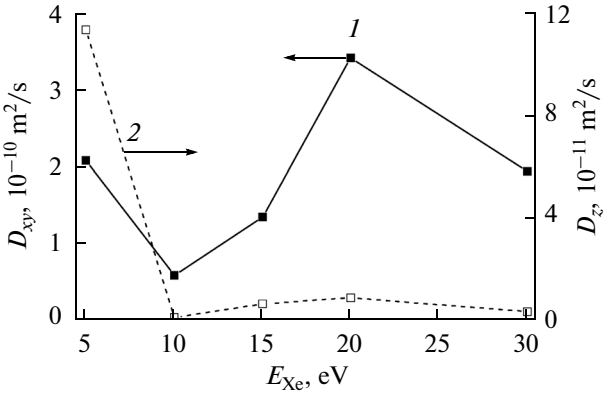

Fig. 3. Horizontal (D_{xy}) and vertical (D_z) components of the Pb atom mobility coefficient obtained as a result of the total bombardment as functions of the bombarding Xe_{13} cluster energies.

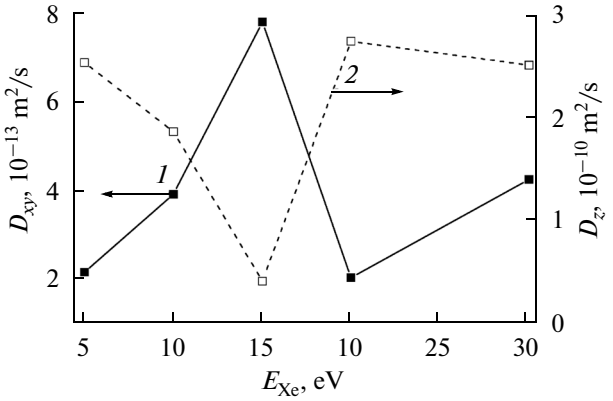

Fig. 4. Horizontal (D_{xy}) and vertical (D_z) components of the C graphene atom mobility coefficient obtained as a result of total bombardment as functions of the bombarding Xe_{13} cluster energies.

in the form of a "honeycomb" and three very weak peaks at angles of 30°, 90°, and 150°, whose origin is due to the presence of divacancies in graphene. Such a pattern of the angular distribution of C atoms was also observed at other energies of bombarding Xe_{13} clusters. The insert in Fig. 2 shows the main peaks of the angular distributions of C atoms in graphene on a magnified scale (in the range of 10°) after bombardment events with energies of 10, 20, and 30 eV. It can be seen that the difference between the forms of the main peaks of the angular distributions for these systems is very insignificant.

The vertical mobility of Pb atoms at energies of bombarding clusters of $E_{Xe} \geq 10$ eV is considerably smaller (by an order or more) than the horizontal mobility (Fig. 3). The horizontal mobility of Pb atoms in the range of energies E_{Xe} under consideration has the form of a sine curve. The maximum of D_{xy} related to significant Pb film loosening is located at $E_{Xe} = 20$ eV, and the minimum, at $E_{Xe} = 10$ eV, where the film was compressed considerably under Xe_{13} cluster impacts. The vertical atom mobility in the Pb film is maximum at energies of bombarding Xe clusters of 5 eV. Individual atomic displacements in the vertical direction increased as a result of such bombardment. But at $E_{Xe} = 10$ eV, the Pb film was compressed and D_z attained its minimum. As E_{Xe} continues to increase, D_z changes insignificantly.

The dependences $D_{xy}(E_{Xe})$ and $D_z(E_{Xe})$ for graphene vary on a mutually compensating basis (Fig. 4); i.e., when D_{xy} increases, D_z decreases, and vice versa. Because of strong interatomic bonds in graphene, the horizontal mobility D_{xy} of C atoms is considerably smaller (by three orders) than the vertical one D_z. The maximum D_{xy} is located at $E_{Xe} = 15$ eV. The minimum D_z corresponds to this energy value. Consequently, the Pb film provides the best protection of graphene against Xe_{13} cluster impacts at this beam energy.

Figure 5 gives the concept of the behavior of the main stresses σ_{zx}, σ_{zy}, and σ_{zz} acting in the metal film plane during bombardment with an energy of $E_{Xe} = 15$ eV. During the first series of bombardments (25 cluster impacts), these stresses decrease gradually to values that are close to zero; i.e., Xe_{13} cluster impacts stimulated structure relaxation in the Pb film. However, as a rule, all subsequent series of impacts increased stresses produced by forces in the horizontal (σ_{zx} and σ_{zy}) and vertical (σ_{zz}) directions. Only the stress σ_{zx} produced during the third series of bombardments was an exception. This bombardment changed the sign of the stress σ_{zx} and did not lead to a significant increase in its value. The behavior of the stresses σ_{zx}, σ_{zy}, and σ_{zz} in the bombarded Pb film depends, of course, on the energy of the bombarding clusters. So, for example, during bombardment with an energy of $E_{Xe} = 5$ eV, significant fluctuations of these stresses specifically were observed during the first series of cluster impacts. As E_{Xe} increased, the considered stresses increased.

These stresses in graphene were quite insensitive to the bombardment duration, but they depended on the energy of the bombarding clusters. This is confirmed, for example, by the distribution of stresses over elementary graphene-sheet areas elongated along the *oy* axis (Fig. 6). This figure shows the distributions obtained under bombardment with an energy of $E_{Xe} = 15$ eV. It can be seen that, for each of the considered σ_{zx}, σ_{zy}, and σ_{zz}, the fluctuations of local stresses obtained after the fifth series of Xe_{13} cluster impacts do not exceed the corresponding characteristics obtained as a result of the first series of impacts. The same relation between the stress amplitudes is also observed for other energies E_{Xe}. The values of the stresses in graphene increase with increasing E_{Xe}. So under bombardment with an energy of $E_{Xe} = 15$ eV, the corresponding local stresses in graphene are two times larger than at $E_{Xe} = 5$ eV.

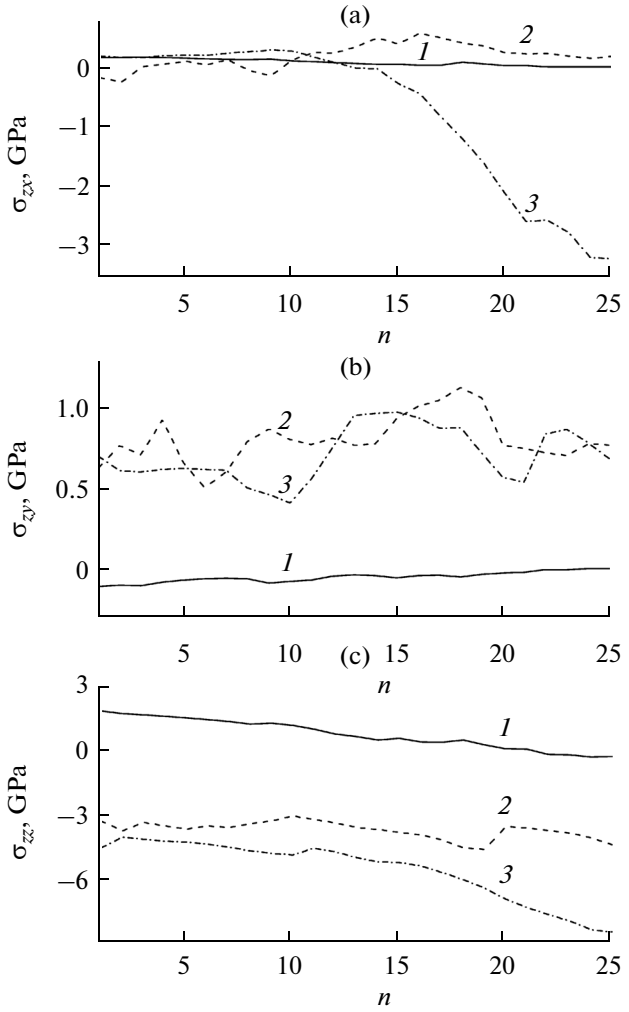

Fig. 5. Evolution of the main stresses in the Pb film upon 15-eV Xe_{13} cluster bombardment of the target: the (*1*) first, (*2*) third, and (*3*) fifth series of impacts and *n* is the number of impacts.

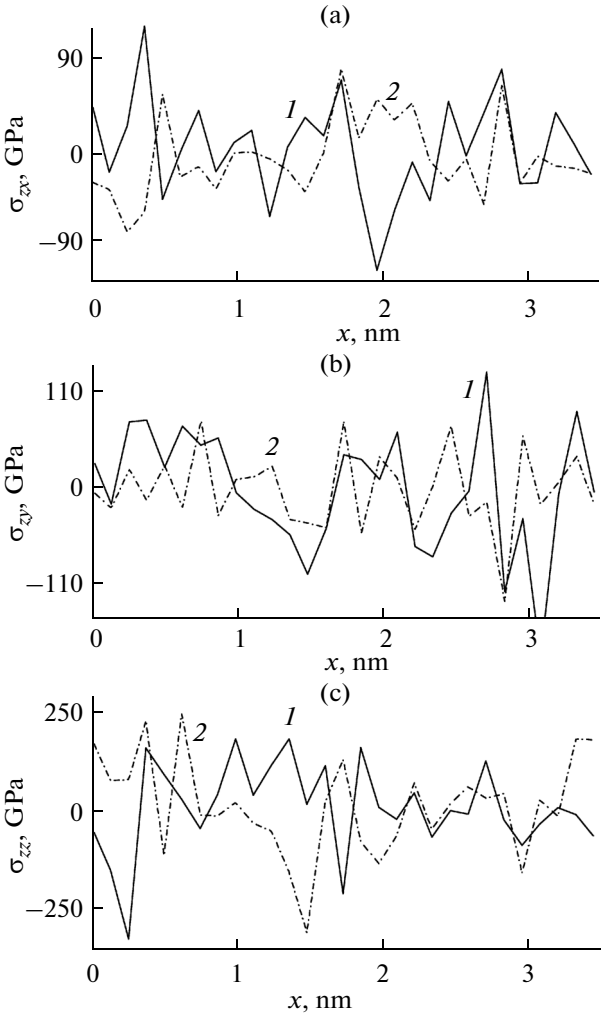

Fig. 6. Distribution of the main stresses in graphene along the "zigzag" direction after 15-eV Xe_{13} cluster bombardment of the target: the (*1*) first and (*2*) fifth series of impacts and *x* is the Cartesian coordinate. The elementary areas are elongated along the *oy* axis.

The dependences of σ_{zx}, σ_{zy}, and σ_{zz} formed in the Pb film on the energy E_{Xe} after all bombardment events are shown in Fig. 7. Each of these stresses increases when passing from 5-eV bombardment of the target to 30-eV cluster bombardment. However, in the interval between these energy values, the behavior of the considered characteristics turns out to be very complicated. The stress σ_{zz}, whose smallest value is at $E_{Xe} = 15$ eV experiences significant oscillations. The largest change in this stress occurs when passing from a bombarding cluster energy of 5 eV to $E_{Xe} = 10$ eV. The increase in E_{Xe} from 20 to 30 eV is accompanied by the largest changes in σ_{zx} and σ_{zy}.

Rather close values of σ_{zx} and σ_{zy} for graphene were obtained in the entire range of energies E_{Xe} under consideration (Fig. 8). The behavior and values of σ_{zz} differ noticeably from analogous characteristics for σ_{zx} and σ_{zy}. As a rule, the values of σ_{zz} are larger than the stresses produced by the horizontal forces, except for the case of $E_{Xe} = 5$ eV. For all three values $\alpha = x, y, z$, the functions $\sigma_{z\alpha}(E_{Xe})$ turn out to be sign-changing. The change in the signs for these functions occurs when E_{Xe} increases from 15 to 20 eV. In addition, the function $\sigma_{zz}(E_{Xe})$ changes its sign once more when passing to an energy of 30 eV. The largest values of σ_{zz} in graphene appear at bombarding cluster energies of 10 and 15 eV.

Graphene attains the largest roughness R_a at a bombarding-cluster energy of 5 eV (Fig. 9). The process of structure relaxation in the Pb film at such an energy was accompanied by a freer transfer of momenta obtained from the Xe_{13} cluster impacts to graphene. In addition, the large incidence angle (75°) made it possible for Xe atoms to reach the graphene surface in the front region even at the initial stage of bombardment. In this case, the decrease in the role of the protective metal film was due to the Xe_{13} cluster incidence angle. For comparison, the dependences

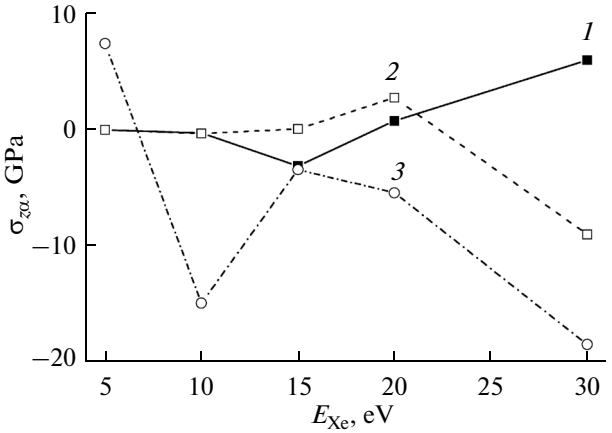

Fig. 7. Main stresses obtained after total bombardment: (*1*) σ_{zx}, (*2*) σ_{zy}, and (*3*) σ_{zz} in the Pb film as functions of the bombarding Xe_{13} cluster energies.

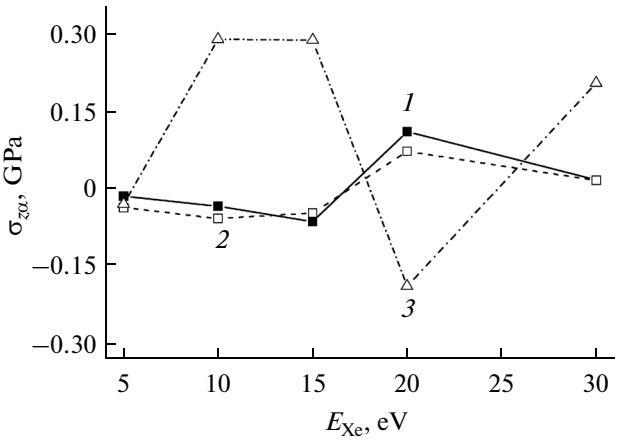

Fig. 8. Main stresses obtained after total bombardment: (*1*) σ_{zx}, (*2*) σ_{zy}, and (*3*) σ_{zz} in graphene as functions of the bombarding Xe_{13} cluster energies.

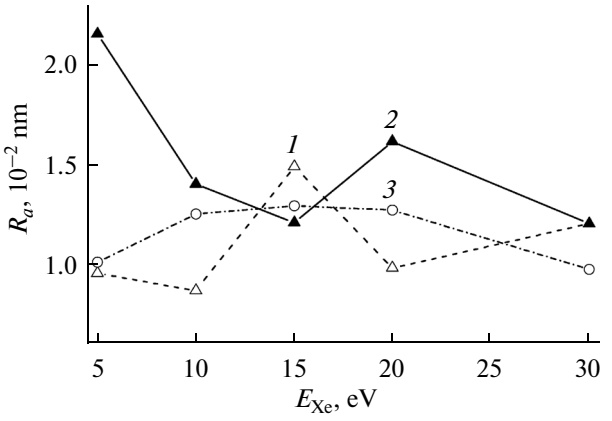

Fig. 9. Dependence of the graphene roughness as functions of the bombarding Xe_{13} cluster energies at incident angles: (*1*) 0°, (*2*) 75°, and (*3*) 90°.

$R_a(E_{Xe})$ obtained as a result of the corresponding bombardments with incidence angles of 0° and 90° are also given in the figure. The values of R_a for graphene at an incidence angle of 75° are larger than at angles of 0° and 90° for almost all values of the energy E_{Xe} in the range under consideration. The case of $E_{Xe} = 15$ eV is an exception. It can be seen that some of the lowest roughness levels were obtained in the cases of vertical and horizontal incidence of clusters with an energy of $E_{Xe} = 5$ eV. The smooth behavior of the function $R_a(E_{Xe})$ was observed only in the case of an incidence angle of 90°, i.e., for "low-level flight."

CONCLUSIONS

Using the molecular dynamics method, we have studied the treatment of a "lead–modified graphene" film by Xe_{13} cluster beams incident at an angle of 75° with an energy ranging from 5 to 30 eV. Complete removal of the Pb film from graphene was observed only after 30-eV cluster bombardment. Graphene with its hydrogenated edges, including divacancy edges, did not acquire visible damage even after 30-eV cluster bombardment. This was confirmed by the forms of the angular distributions of the nearest geometric neighbors in graphene obtained as a result of bombardment. The dependence of the horizontal component of the Pb-atom mobility coefficient on the energies of bombarding Xe_{13} clusters had the form of a sine curve, while the corresponding vertical component retained low values up to a cluster energy of 30 eV after a sharp decrease at $E_{Xe} = 10$ eV. Analogous components for graphene exhibited an oscillating character with increasing E_{Xe}. In this case, their change occurs in opposite directions to each other. Among the main components of the stresses in the Pb film, only σ_{zx} tended stably to decreasing value during bombardment, while the behavior of the components σ_{zy} and σ_{zz} were evidence of the presence of a tendency for the corresponding stresses to accumulate with time. The distributions of the main stresses in graphene did not yield the enhancement of fluctuations when passing to each new series of bombardments. The most significant total stresses in the Pb film appeared after bombardment with an energy of $E_{Xe} = 30$ eV. In the case of graphene, another regularity was observed: among the main stresses, the largest component σ_{zz} had its maxima at $E_{Xe} = 10$ and 15 eV. The graphene roughness turned out to be maximum at a bombarding-cluster energy of 5 eV, at which the vertical mobility of C atoms attained one of its largest values and all three components of the stresses in the graphene plane had very small values at the same time. For almost all E_{Xe} under study, the values of R_a obtained under bombardment at a cluster-incidence angle of 75° were larger than under bombardment with a beam of analogous clusters at incident angles of 0° and 90°.

ACKNOWLEDGMENTS

This work was supported by the Russian Foundation for Basic Research (grant no. 13-08-00273).

REFERENCES

1. P. Sutter and E. Sutter, Adv. Funct. Mater. **23**, 2617 (2013).
2. S. Nie, N. C. Bartelt, J. M. Wofford, O. D. Dubon, K. F. McCarty, and K. Thurmer, Phys. Rev. B: Condens. Matter **85**, 205406 (2012).
3. J. M. Wofford, E. Starodub, A. L. Walter, S. Nie, A. Bostwick, N. C. Bartelt, K. Thurmer, E. Rotenberg, K. F. McCarty, and O. D. Dubon, New J. Phys. **14**, 053008 (2012).
4. A. E. Galashev and V. A. Polukhin, J. Surf. Invest.: X-ray, Synchrotr. Neutron Tech. **8** (5), 1078 (2014).
5. A. E. Galashev and V. A. Polukhin, Phys. Met. Metallogr. **115**, 697 (2014).
6. A. E. Galashev and O. R. Rakhmanova, Phys. Usp. **57**, 970 (2014).
7. A. E. Galashev and A. A. Galasheva, High Energy Chem. **48**, 112 (2014).
8. T. Matsuur, J. Murota, and Y. Sawada, Appl. Phys. Lett. **63**, 2803 (1993).
9. H. Feil and J. Dieleman, J. Appl. Phys. **74**, 1303 (1993).
10. M. V. Ramana Murty and Y. A. Atwater, Phys. Rev. B **45**, 1507 (1992).
11. J. Tarus, K. Nordlund, A. Kuronen, and J. Keinonen, Phys. Rev. B **58**, 9907 (1998).
12. K. E. Ryan and B. J. Garrison, Anal. Chem. **80**, 5302 (2008).
13. H. Gao, J. Zhou, M. Lu, W. Fa, and Y. Chen, J. Appl. Phys. **107**, 114311 (2010).
14. D. Ma and Z. Yang, New J. Phys. **13**, 123018 (2011).
15. Y. Watanabe, H. Yamaguchi, M. Hashinokuchi, K. Sawabe, S. Maruyama, Matsumoto and Y. K. Shobatake, Chem. Phys. Lett. **413**, 331 (2005).
16. J. Tersoff, Phys. Rev. Lett. **61**, 2879 (1988).
17. S. J. Stuart, A. V. Tutein, and J. A. Harrison, J. Chem. Phys. **112**, 6472 (2000).
18. H. Rafii-Tabar, Phys. Rep. **325**, 239 (2000).
19. Y. M. Kim and S.-C. Kim, J. Korean Phys. Soc. **40**, 293 (2002).
20. A. Arkundato, Z. Su'ud, M. Abdullah, and W. Sutrisno, Int. J. Appl. Phys. Math. **3**, 1 (2013).
21. F.-Y. Li and R. S. Berry, J. Phys. Chem. **99**, 2459 (1995).
22. J. F. Ziegler, J. P. Biersack, and U. Littmark, *Stopping and Ranges of Ions in Matter* (Pergamon, New York, 1985), V. 1.
23. A. Delcorte and B. J. Garrison, J. Phys. Chem. B **104**, 6785 (2000).
24. F. D. Lamari and D. Levesque, Carbone **49**, 5196 (2011).
25. H. J. C. Berendsen, J. P. M. Postma, W. F. van Gunsteren, A. DiNola, and J. R. Haak, J. Chem. Phys. **81**, 3684 (1984).
26. A. E. Galashev, Fiz. Mezomekh. **17**, 67 (2014).
27. A. Y. Galashev and O. R. Rakhmanova, Chin. Phys. B **24**, 020701 (2015).
28. A. Y. Galashev, Comp. Mater. Sci. **98**, 123 (2015).
29. S. Yu. Davydov, Phys. Solid State **54**, 875 (2012).
30. Z. H. Jin, H. W. Sheng, and K. Lu, Phys. Rev. B **60**, 141 (1999).

Translated by L. Kulman